doi:10.1038/nature10348

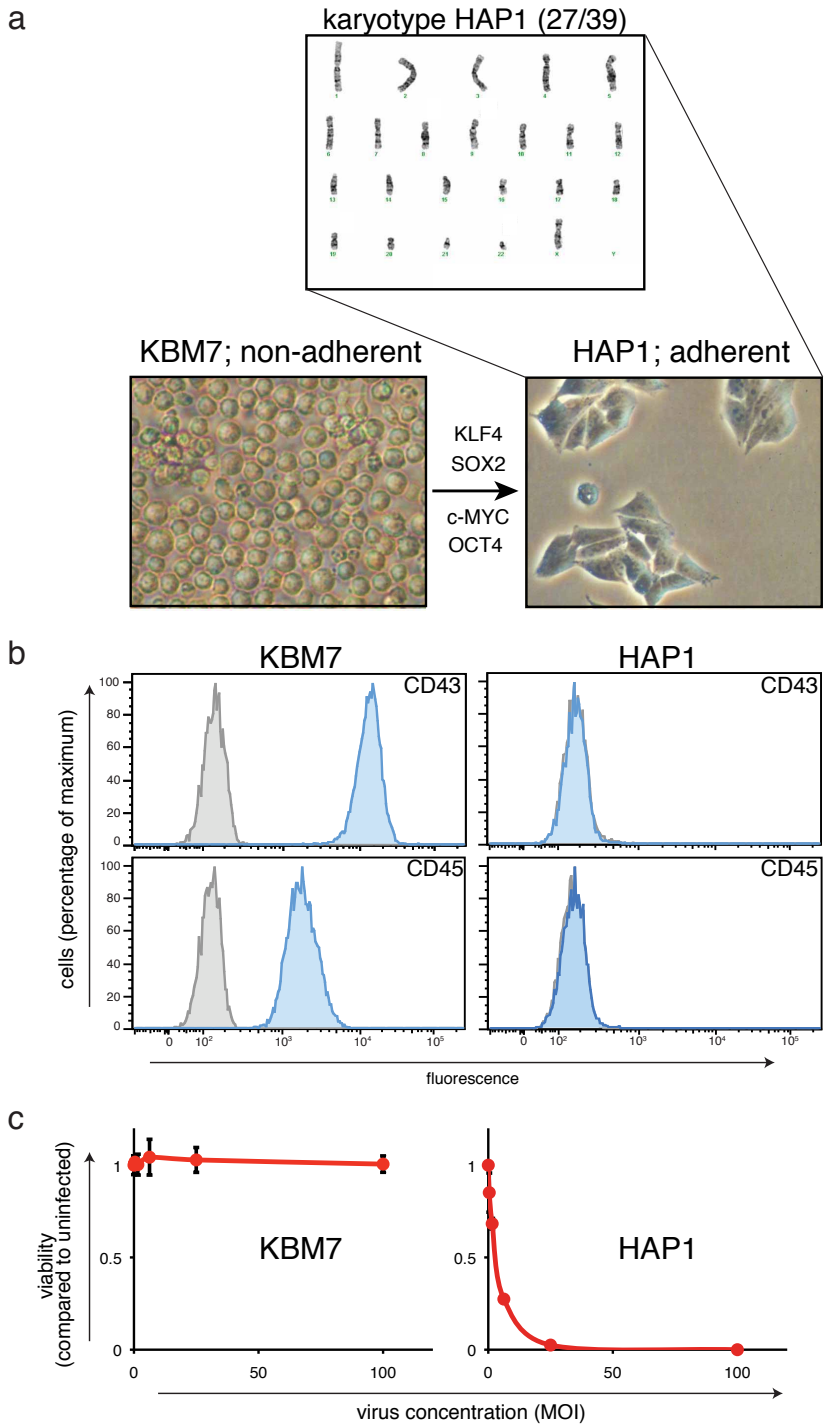

Supplemental Figure 1. Generation of HAP1 cells and susceptibility to rVSV-GP-EboV. **a**, Near-haploid KBM7 cells were coinfected with retroviral vectors expressing OCT4/ SOX2/c-MYC and KLF4 and an adherently growing subclone was identified (HAP1 cells). Karyotypic analysis of HAP1 cells indicates that the majority of cells (27 out of 39 analyzed) is haploid for all chromosomes **b**, Staining of KBM7 cells and HAP1 cells with pan-hematopoietic markers CD43 and CD45. Stained cells were examined by flow-cytometry. The unstained control is indicated in grey. **c**. Susceptibility of HAP1 and KBM7 cells to cell-killing by rVSV-GP-EboV.

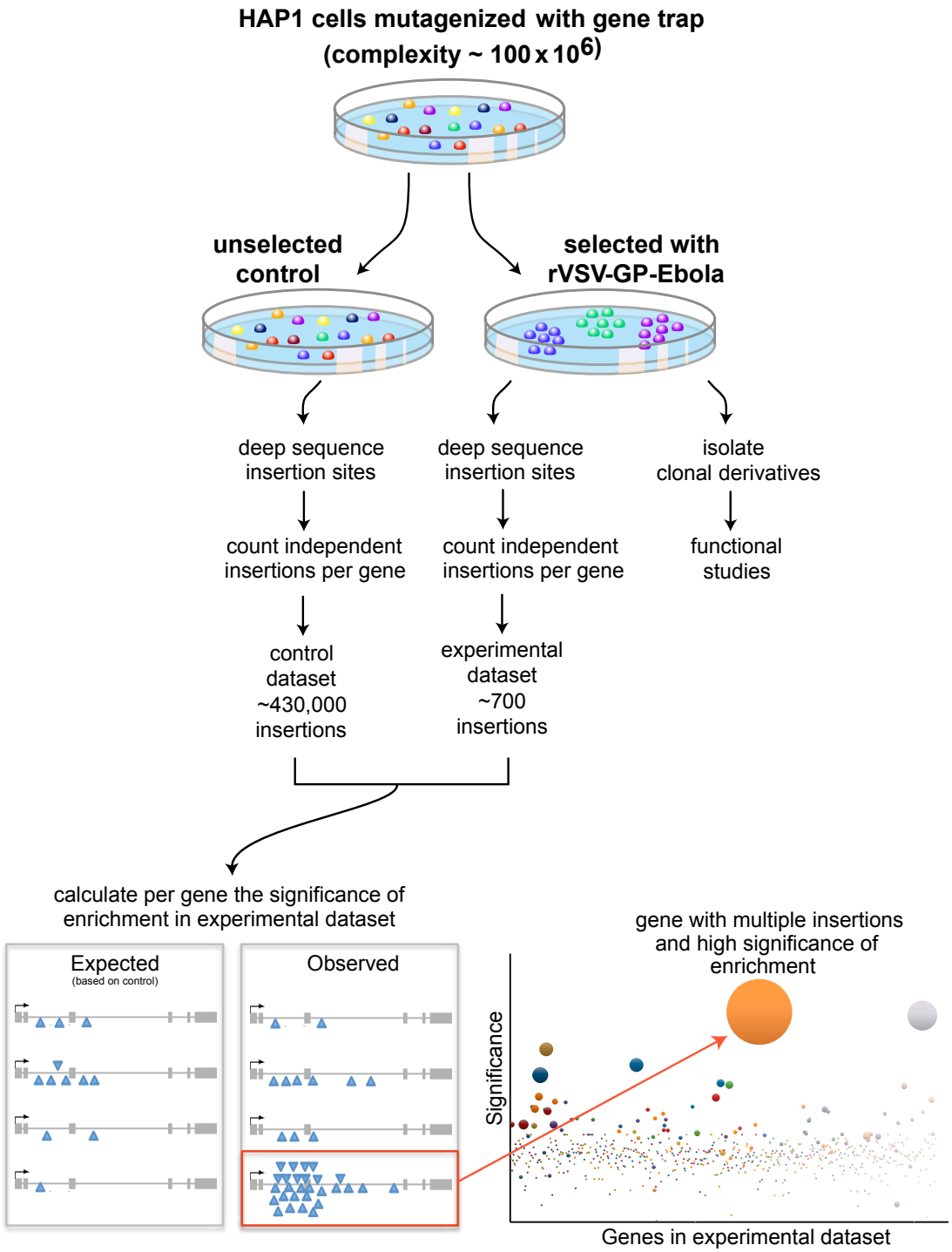

Supplemental Figure 2. Outline of the haploid genetic screen to identify host factors for Ebola virus entry. 100 million early passage HAP1 cells were infected with gene-trap virus and further expanded. A subset of cells was used to characterize the distribution of gene-trap insertion across the human genome. Sequences flanking the gene-traps were amplified, sequenced in parallel and aligned to the human genome. Independent insertion events into annotated genes were counted. 100 million cells were infected with rVSV-GP-EboV virus and resistant clones were pooled and expanded. Most of these cells were used to amplify sequences flanking the gene-traps, sequence the insertion sites in parallel, and align these sequences to the human genome. A subset of the cells was used to obtain $NPC1^{GT}$ and $VPS33^{GT}$ cells through subcloning. Gene disruption events in the selected population were compared to the unselected cell population and genes that were significantly enriched for mutations were identified.

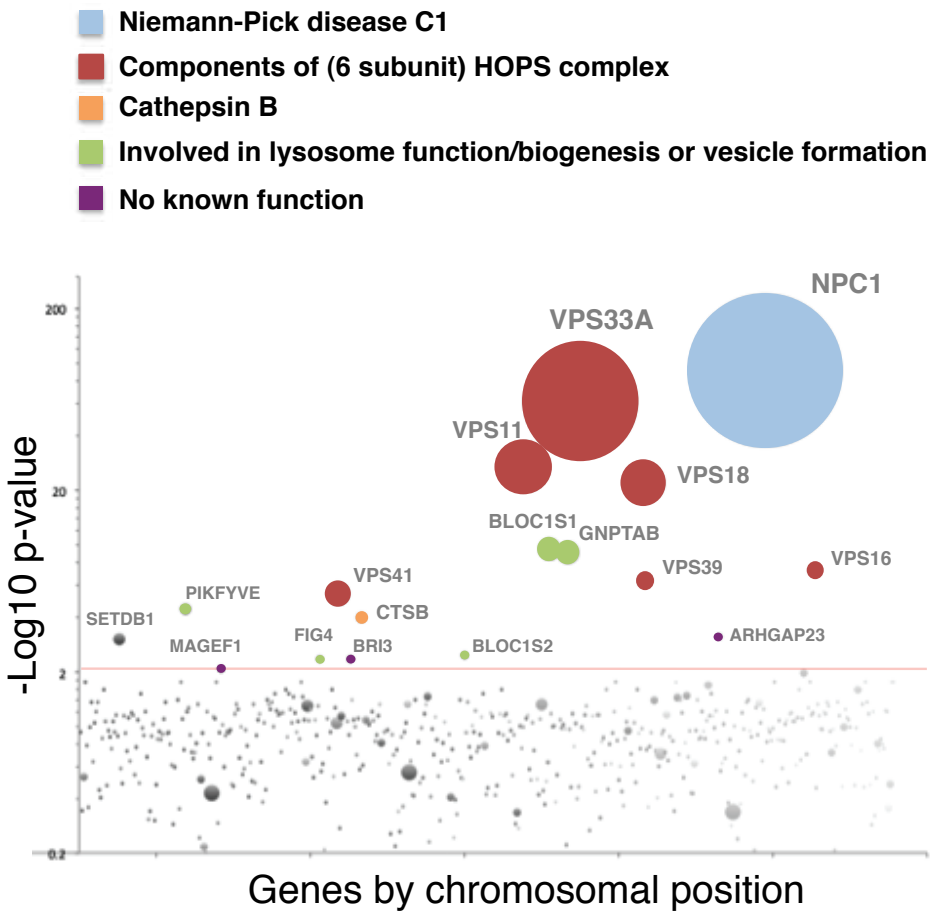

Supplemental Figure 3. Classes of genes that are required for rVSV-GP-EboV induced cytotoxicity. Significant hits were labeled according to the following annotation: Niemann-Pick disease C1, lysosomal cholesterol transporter (blue), component of 6-subunit HOPS complex (red), cathepsin B (orange), involved in lysosome function /biogenesis (green) or having no known function (purple).

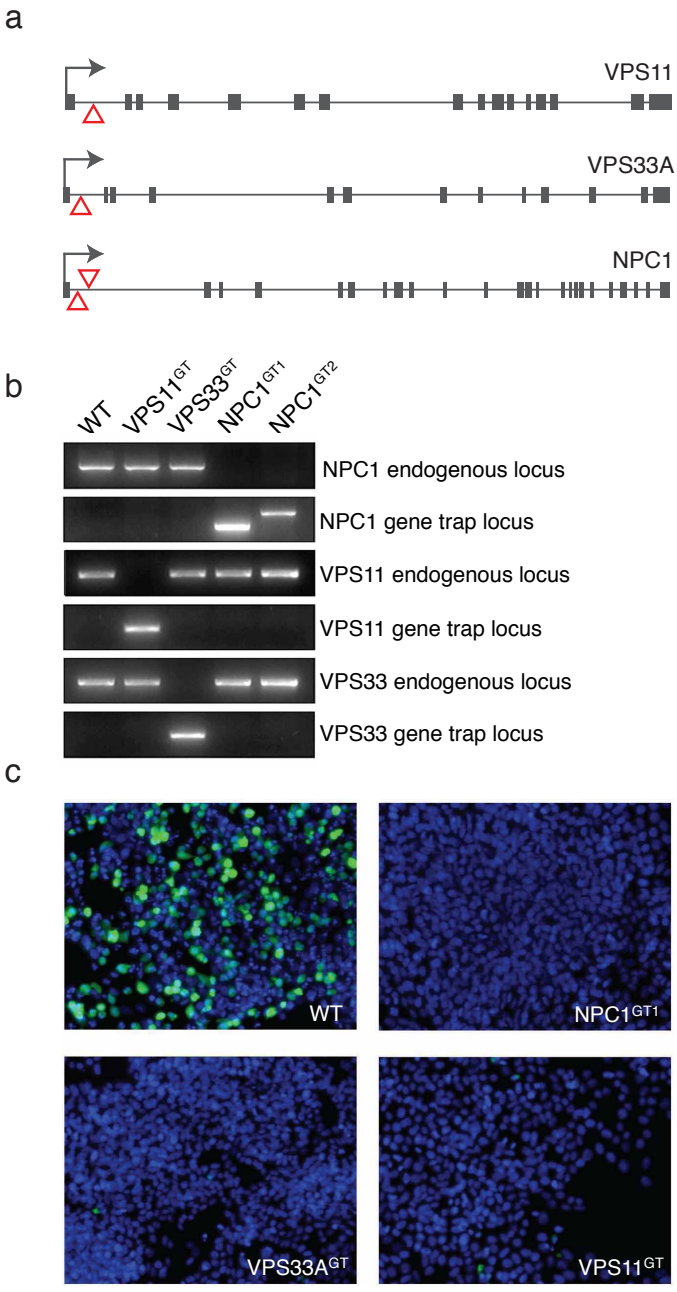

Supplemental Figure 4. Identification and characterization of HAP1 cells carrying gene-trap insertions in the NPC1, VPS11 and VPS33A loci. **a**, Schematic outline of the positions of gene-trap insertions in the corresponding genes. Gene-traps were located in the sense orientation in intronic sequences of the 5'-end of the gene and are therefore predicted to disrupt gene function. **b**, Clonal cell lines carrying the gene-trap insertions in the corresponding loci were identified through subcloning. Genotyping indicates the absence of wild type genomic loci and the presence of gene-trap loci. **c**, Cells carrying gene-trap insertions in the corresponding loci and wild type HAP1 cells were inoculated with rVSV-GP-EboV, and infected cells (green) were visualized by fluorescence microscopy 12 h later.

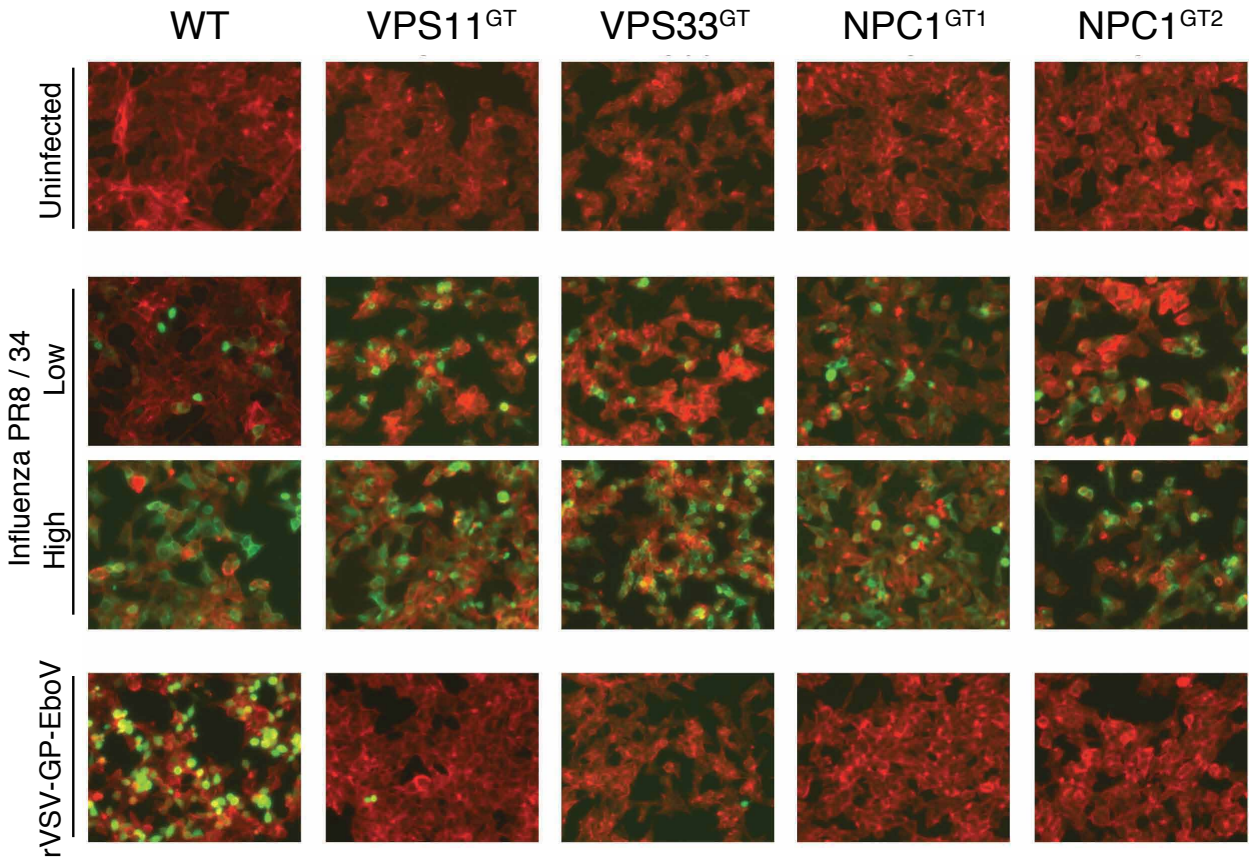

Supplemental Figure 5. Susceptibility of NPC1 and HOPS mutant cell lines to influenza A virus infection. Cells were infected with influenza A/PR8/34 virus (two different MOIs), or VSV-GP-EboV. Influenza virus-infected cells (green) were stained 11 h later with antibodies directed against the viral nucleoprotein and visualized by fluorescence microscopy. rVSV-GP-EboV-infected cells (green) were imaged by eGFP fluorescence. Cells were counterstained with a β-actin-specific antibody (red).

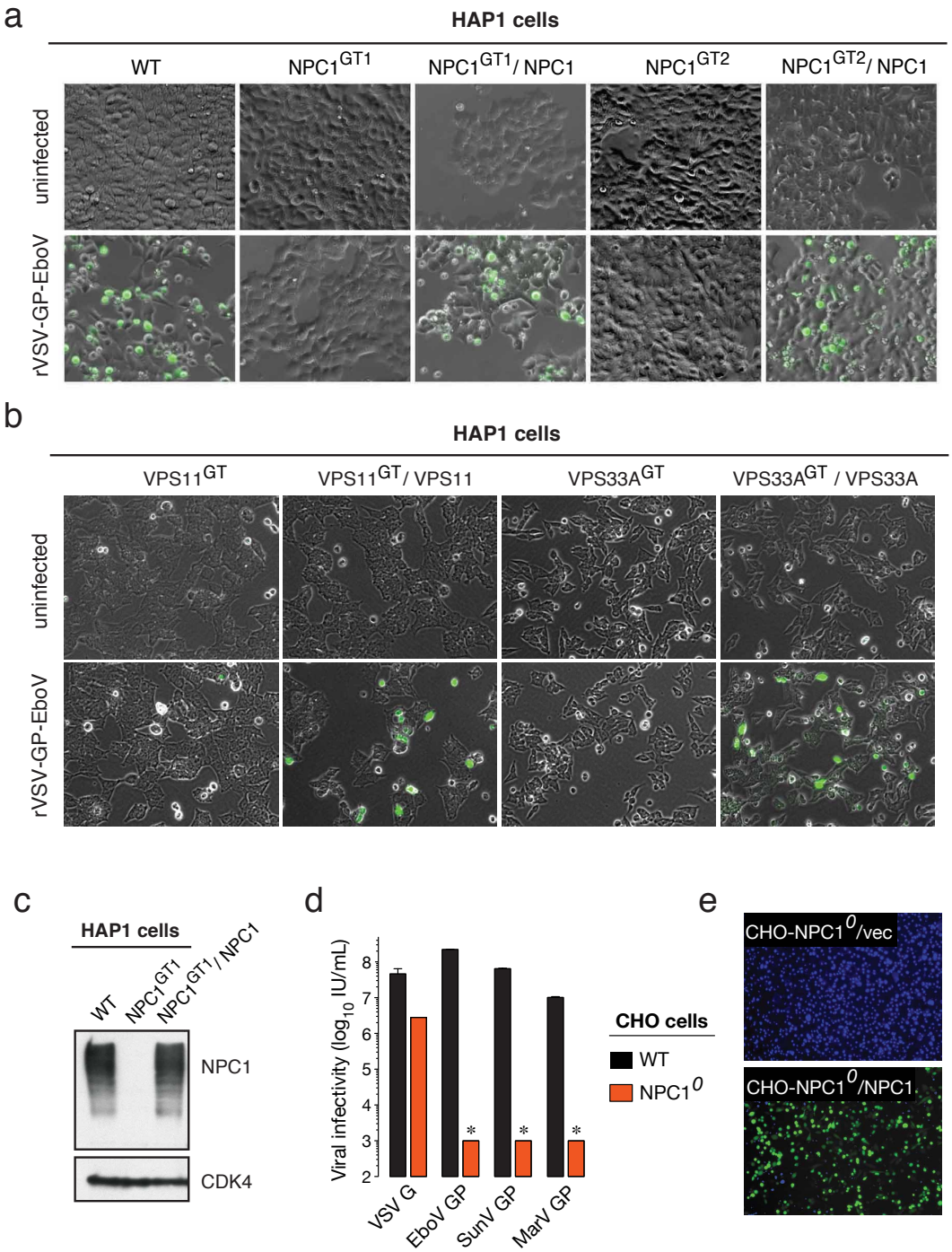

Supplemental Figure 6. Loss of NPC1, VPS11, or VPS33A confers resistance to viral infection mediated by the Ebola virus glycoprotein that can be restored by exogenous expression of the respective host gene. **a**, HAP1 cells carrying independent gene-trap insertions in the NPC1 locus were infected with a retroviral vector directing the expression of NPC1, or with a control virus. Cells were then infected with rVSV-GP-EboV, and eGFP-positive infected cells (green) were visualized 12 h later by fluorescence microscopy. Overlaid differential-interference contrast (DIC) and fluorescence micrographs of the same fields are shown. **b**, HAP1 cells carrying gene-trap insertions in the VPS11 and VPS33A locus were infected with a retroviral vector directing the expression of the corresponding cDNAs, or with a control virus. Cells were treated as in panel a. **c**, Immunoblot blot analysis of NPC1 in HAP1 cells, HAP1 cells carrying a gene-trap insertion in the NPC1 locus and the same cell line infected with the NPC1-expressing retrovirus. CDK4 was used a loading control. **d**, Wild type or NPC1-deficient CHO cells were challenged with VSV pseudotyped with the indicated viral glycoproteins, and viral infectivity was measured 24 h later. **e**, NPC1-deficient CHO cells were infected with a retroviral vector directing the expression of NPC1, or with a control virus. Cells were then infected with rVSV-GP-EboV, and eGFP-positive infected cells were visualized by fluorescence microscopy 14 h later.

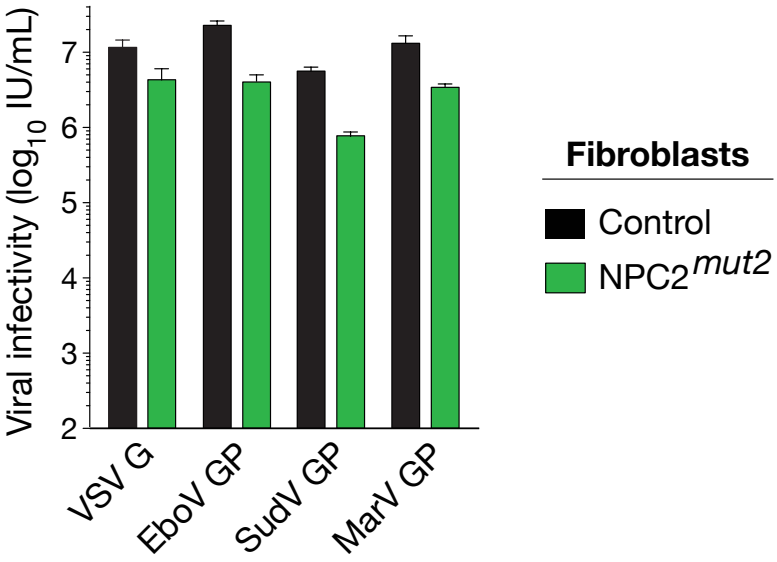

Supplemental Figure 7. NPC2-mutant fibroblasts derived from a second Niemann-Pick patient are susceptible to viral infection mediated by the Ebola virus glycoprotein. Fibroblasts from an apparently normal individual and a Niemann-Pick patient carrying homozygous mutations in NPC2 were infected with VSV pseudotypes bearing the indicated viral glycoproteins, and viral infectivity was measured 24 h later. Means ± standard deviation (SD) are shown.

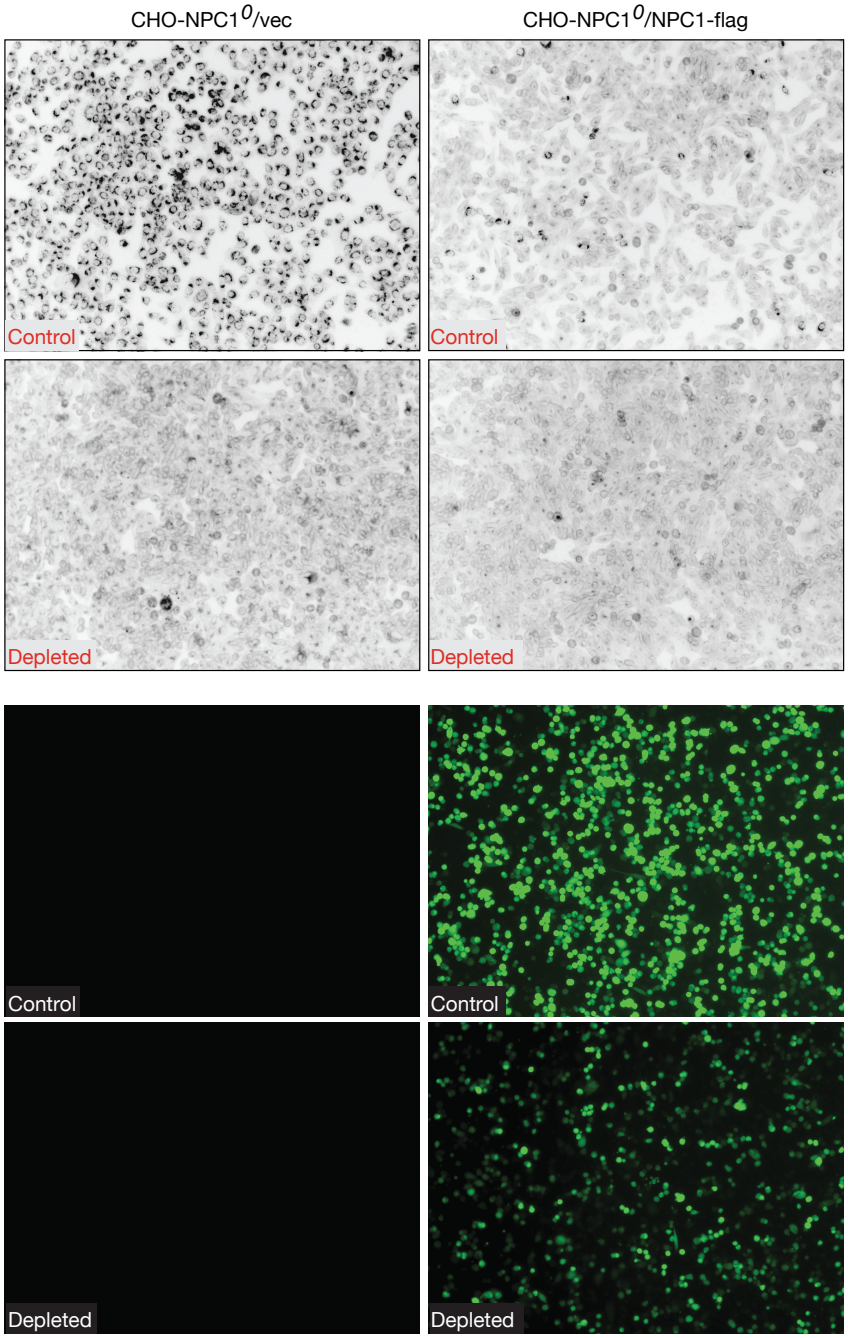

Supplemental Figure 8. Clearance of accumulated cholesterol does not render NPC1-deficient cells susceptible to infection by rVSV-GP-EboV. Wild type and NPC1-null CHO cells were cultivated either in normal growth medium (control) or in growth medium containing lipoprotein-depleted fetal bovine serum for 6 days. Cells were then stained with filipin to visualize accumulated cholesterol (top panels) or infected with rVSV-GP-EboV (bottom panels). Filipin-stained (black) or infected cells (green) were visualized by fluorescence microscopy.

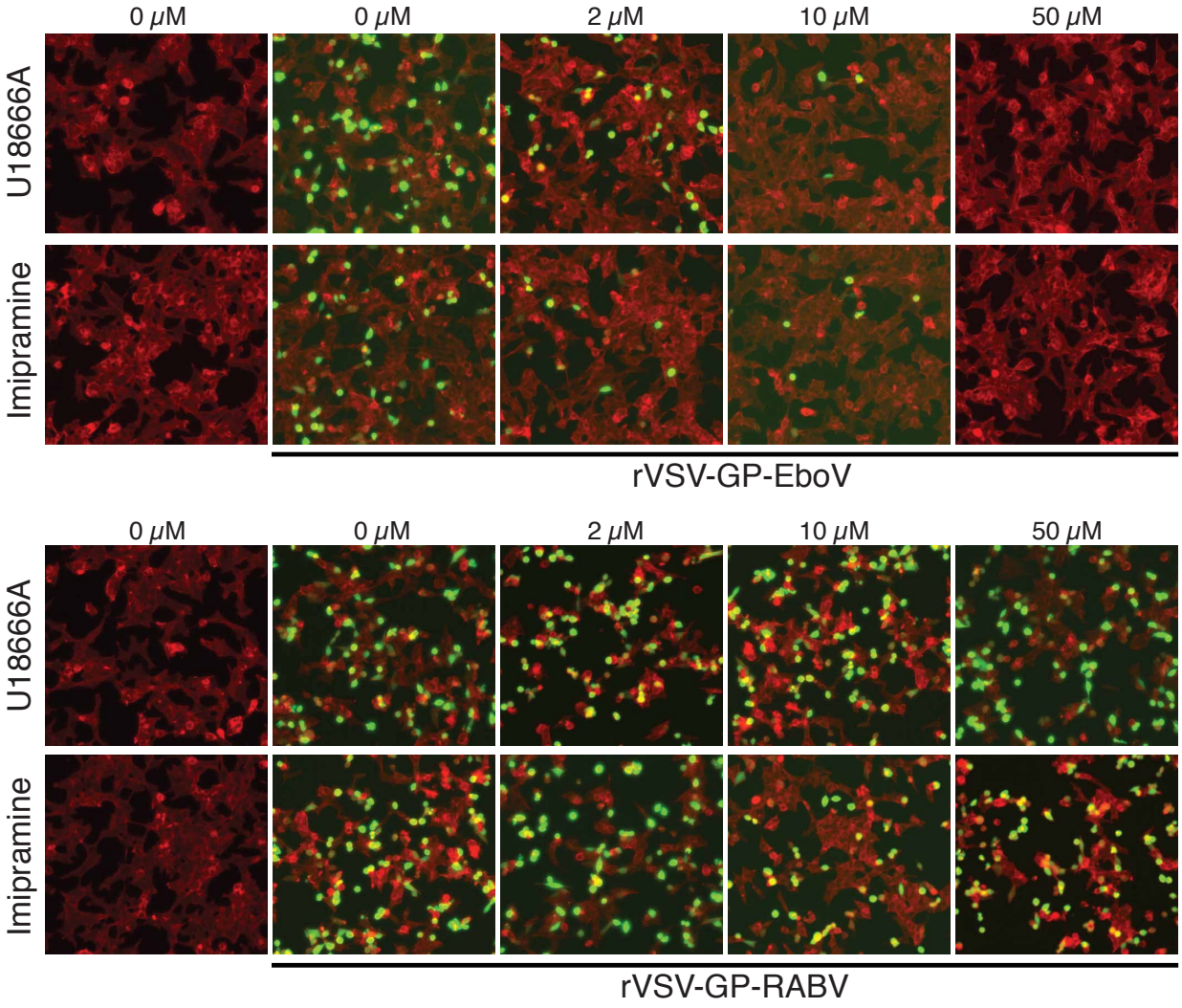

Supplemental Figure 9. Viral infection mediated by the Ebola glycoprotein is inhibited by imipramine and U18666A. HAP1 cells were pretreated for 30 minutes with the indicated concentrations of U18666A or the anti-depressant imipramine and then infected with rVSV-GP-EboV or rVSV-G-RABV carrying a GFP transgene. eGFP-positive infected cells were visualized by fluorescence microscopy 8 h later. Cells were counterstained with β-actin (red).

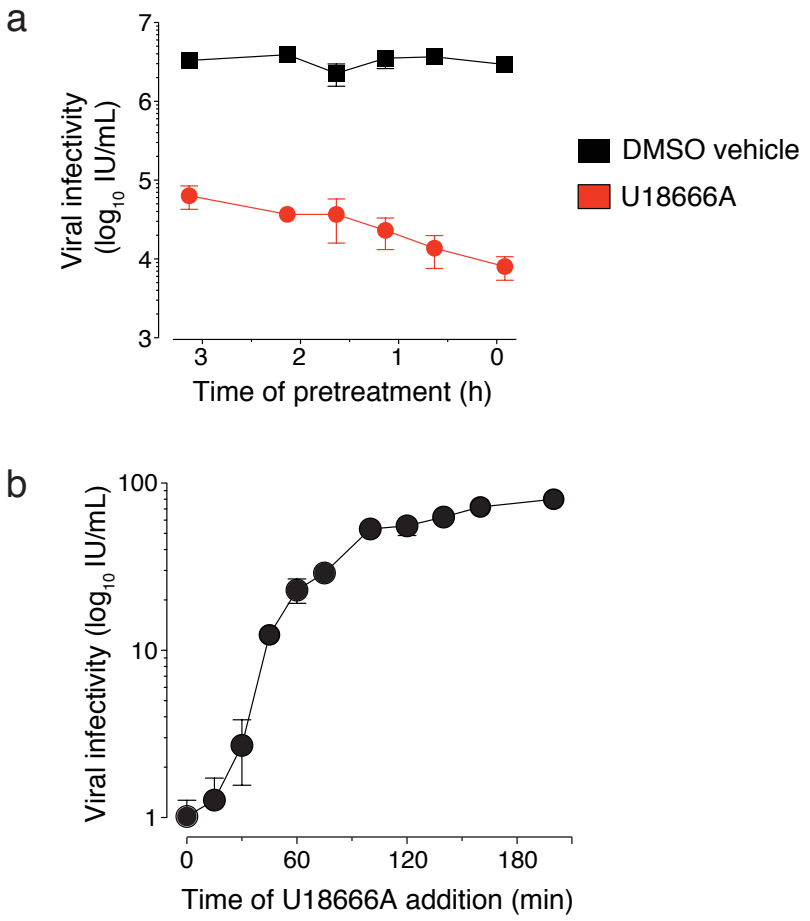

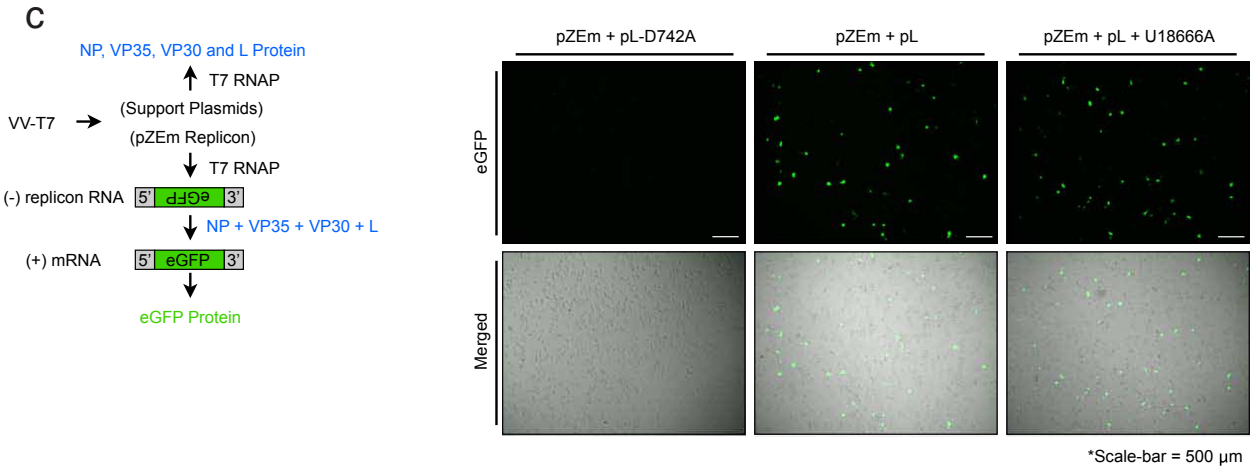

Supplemental Figure 10. U18666A acts rapidly to inhibit Ebola virus GP-dependent entry and does not affect the cytoplasmic steps of Ebola viral replication. **a**, Vero cells were left untreated or were pretreated with U18666A (20 µM) for the indicated times and then infected with rVSV-GP-EboV in the presence of U18666A. After 1 h, viral entry was terminated by addition of NH4Cl (20 mM). Viral infectivity was measured 12-14 h later. **b**, Vero cells were exposed to VSV-GP-EboV virus for 1 h at 4˚C, washed to remove unbound inoculum, and then incubated in growth medium at 37˚C. At the indicated times post-warming, growth medium containing U18666A (20 µM final) was added. Viral infectivity was measured 16 h later. Means ± standard deviation (SD) are shown. **c**, T7 RNA polymerase drives the production of the Ebola virus replication proteins (NP, VP35, VP30 and L) from individual plasmids with T7 promoters. Additionally, T7 RNAP produces a negative-sense viral genome analogue RNA from the replicon plasmid (pZEm) that encodes eGFP. The viral polymerase machinery utilizes the replicon RNA as a transcription template to produce a positive-sense eGFP mRNA resulting in eGFP protein production. A single amino-acid substitution to the active site of the RdRP domain within L abolishes replicon activity and eGFP production and serves as negative control.

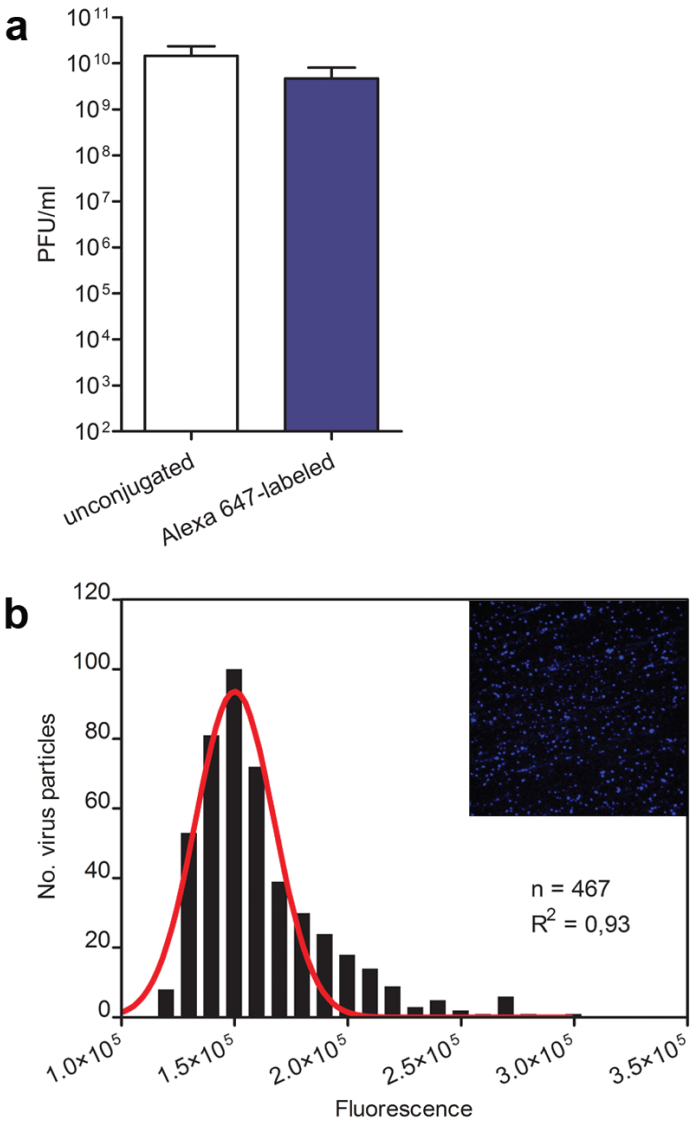

Supplemental Figure 11. Alexa Fluor 647 conjugation to rVSV-GP-EboV particles does not affect infectivity. **a**, rVSV-GP-EboV titers following Alexa 647 conjugation as determined by plaque assay. Means ± standard deviation (SD) are shown (n = 3). **b**, Net fluorescence intensity of Alexa 647-labeled rVSV-GP-EboV particles. Virions on a glass coverslip were imaged by confocal fluorescence microscopy, and the fluorescence intensity (arbitrary units) of each particle was measured. The distribution of particle fluorescence intensities is depicted as a histogram plot in which the red line shows the best-fit Gaussian curve. The inset shows a representative image of virus particles (blue).

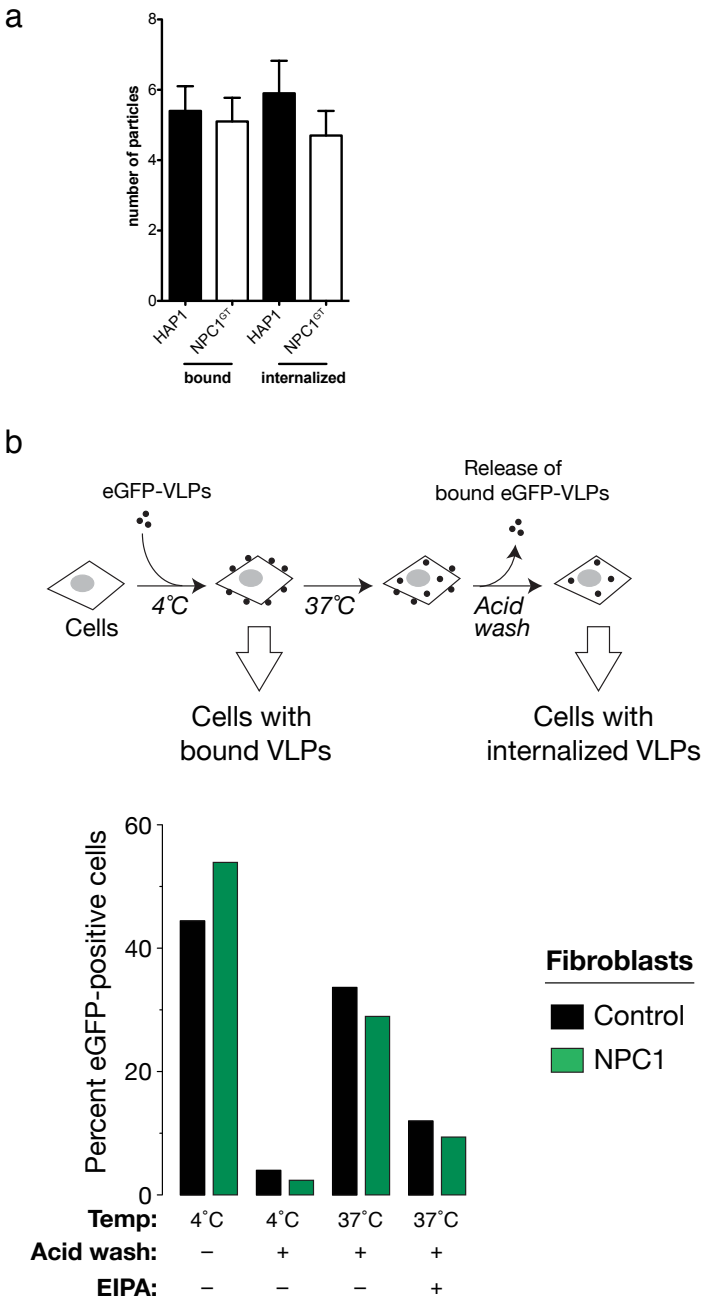

Supplemental Figure 12. Quantification of viral attachment and internalization in NPC1-deficient HAP1 cells and NPC1-mutant fibroblasts. **a**, Ten individual cells of the experiment described in the legend of Figure 3A were used for quantification of bound/internalized viral particles. Briefly, the indicated HAP1 clones were infected with Alexa 647-labeled rVSV-GP-EboV at 4°C. Non-internalized, bound viral particles were stained with a GP-specific antibody. Internalization of virus was assessed by warming cells to 37°C for 2 h. Cells were counterstained with Alexa 594-wheat germ agglutinin to outline the plasma membrane. Viral particles were counted using Slidebook 4.2 software (Intelligent Imaging Innovations; Denver, CO). **b**, Virus-like particles (VLPs) containing the EboV matrix protein VP40 fused to the enhanced green fluorescent protein (eGFP-VP40) were generated as described previously. Binding and internalization of VLPs in control and NPC1-mutant fibroblasts was assessed as follows. Cells were exposed to VLPs (1–2 μg protein/well) by centrifugation at 250 x g and 4˚C for 1 h, washed with PBS, and fixed with paraformaldehyde (PFA). The degree of VLP binding (eGFP signal sensitive to a brief acid wash at pH 3.0) was quantitated by flow cytometry. To allow viral internalization, some samples were shifted to 37˚C for 3 h after the 4˚C step, and then washed and fixed as described above. The degree of VLP internalization (eGFP signal resistant to a brief acid wash at pH 3.0) was quantitated by flow cytometry. VLP internalization into control and NPC1-mutant fibroblasts was sensitive to preincubation of cells with EIPA (50 μM), as observed in other cell types. Averages of two trials from a representative experiment are shown.

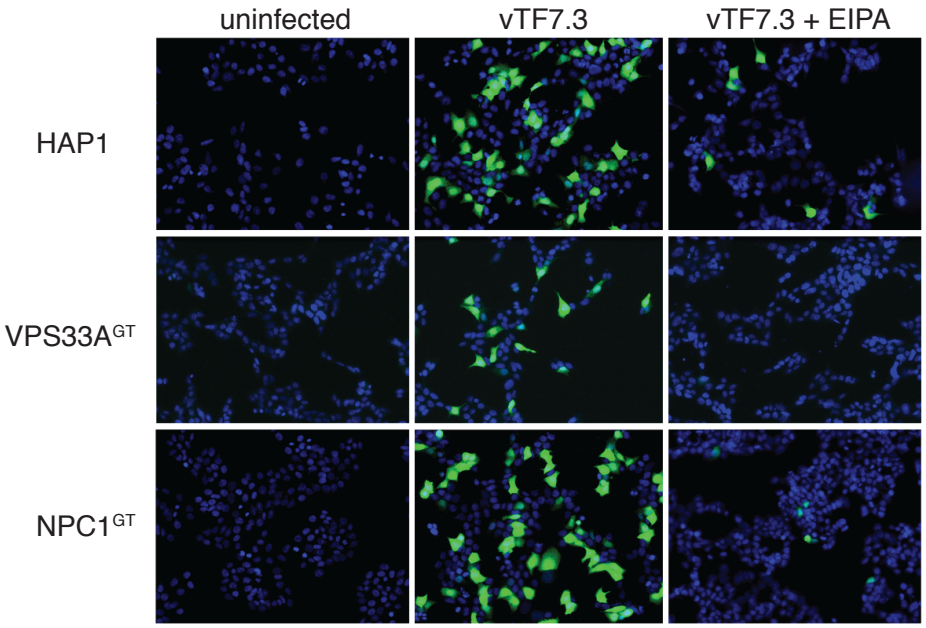

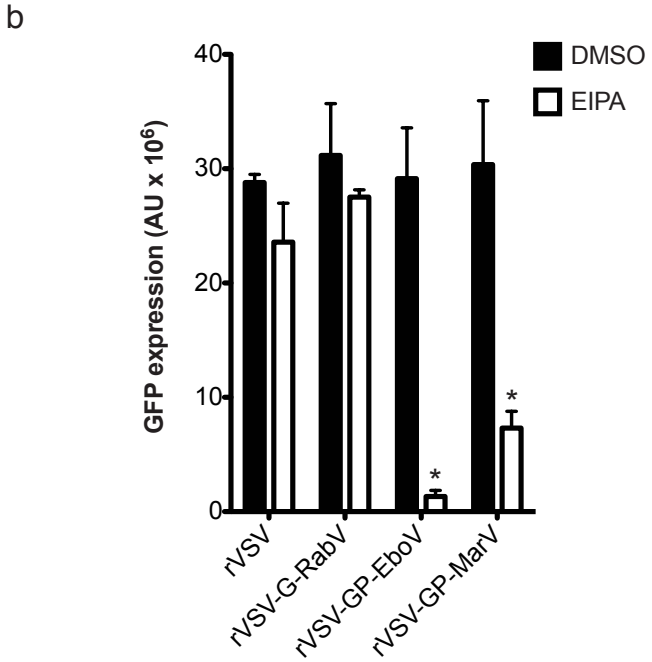

Supplemental Figure 13. HOPS- and NPC1-deficient cells support entry of vaccinia virus, which is internalized by macropinocytosis. **a**, The indicated HAP1 clones were inoculated with a vaccinia virus expressing T7 polymerase (vTF7.3) for 1 h at 37°C in PBS in the absence or presence of 50 μM EIPA. As a control, cells were inoculated with PBS alone. Subsequently, all cells were transfected with a plasmid encoding GFP (green) under control of a T7 promoter. 4 h after transfection cells were fixed with 4% PFA at RT and the nuclei were stained with DAPI (blue). Fluorescence images were acquired and representative images are indicated. **b**, HAP1 cells were challenged with the indicated viruses (MOI 10) in the absence or presence of 50 μM EIPA. GFP expression was quantified 8 h post inoculation by using a Typhoon 9400 Fluorescent Imager (GE Healthcare). The data are presented in arbitrary units (AU). Means ± standard deviation (SD) are indicated.

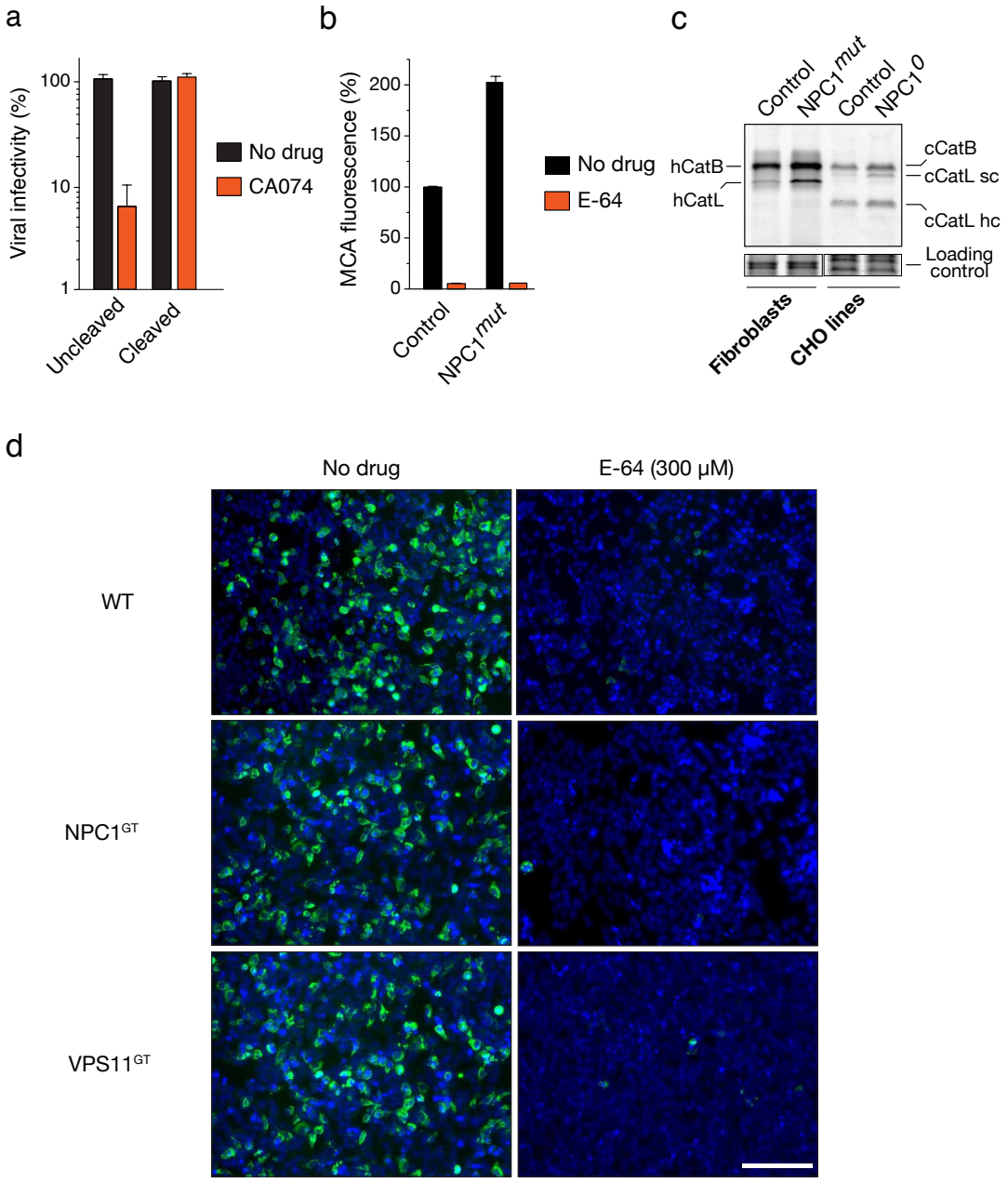

Supplemental Figure 14. The activities of endosomal cysteine cathepsins B and L are not inhibited in NPC1-defective cells. **a**, In vitro cleaved rVSV-GP-EboV bypasses the intracellular requirement for cathepsin B (CatB). Infectivity of mock- or thermolysin-cleaved rVSV-GP-EboV in Vero cells treated with the CatB inhibitor CA074. **b**, Fibroblasts from an apparently normal individual (control) and a Niemann-Pick patient carrying homozygous mutations in NPC1 were lysed at acid pH, and the capacity of these acidic extracts to cleave a fluorogenic peptide substrate for CatB and CatL was measured (see Supplementary Methods for details). Pretreatment of cell extracts with the pan-cysteine protease inhibitor E-64 abolished substrate cleavage, confirming that only cysteine cathepsin activities were being measured. **c**, Intact control and NPC1-deficient fibroblasts and CHO cells were incubated with a cell-permeable fluorophore-tagged suicide substrate that covalently attaches to key catalytic residues in CatB/CatL, a process that requires enzyme activity. Cells were then lysed and fluorophore-labeled CatB and CatL proteins were detected by SDS-polyacrylamide gel electrophoresis and fluorescence imaging. hCatB and hCatL, human enzymes. cCatB and cCatL, CHO enzymes. sc and hc, single chain and heavy chain forms of CatL. **d**, The indicated HAP1 clones were pre-treated with the pan-cysteine cathepsin inhibitor E-64 (300 μM) and then exposed to reovirus T1L virions (MOI 1). Cells were fixed at 24 h post-infection and immunostained for the viral non-structural protein σNS.

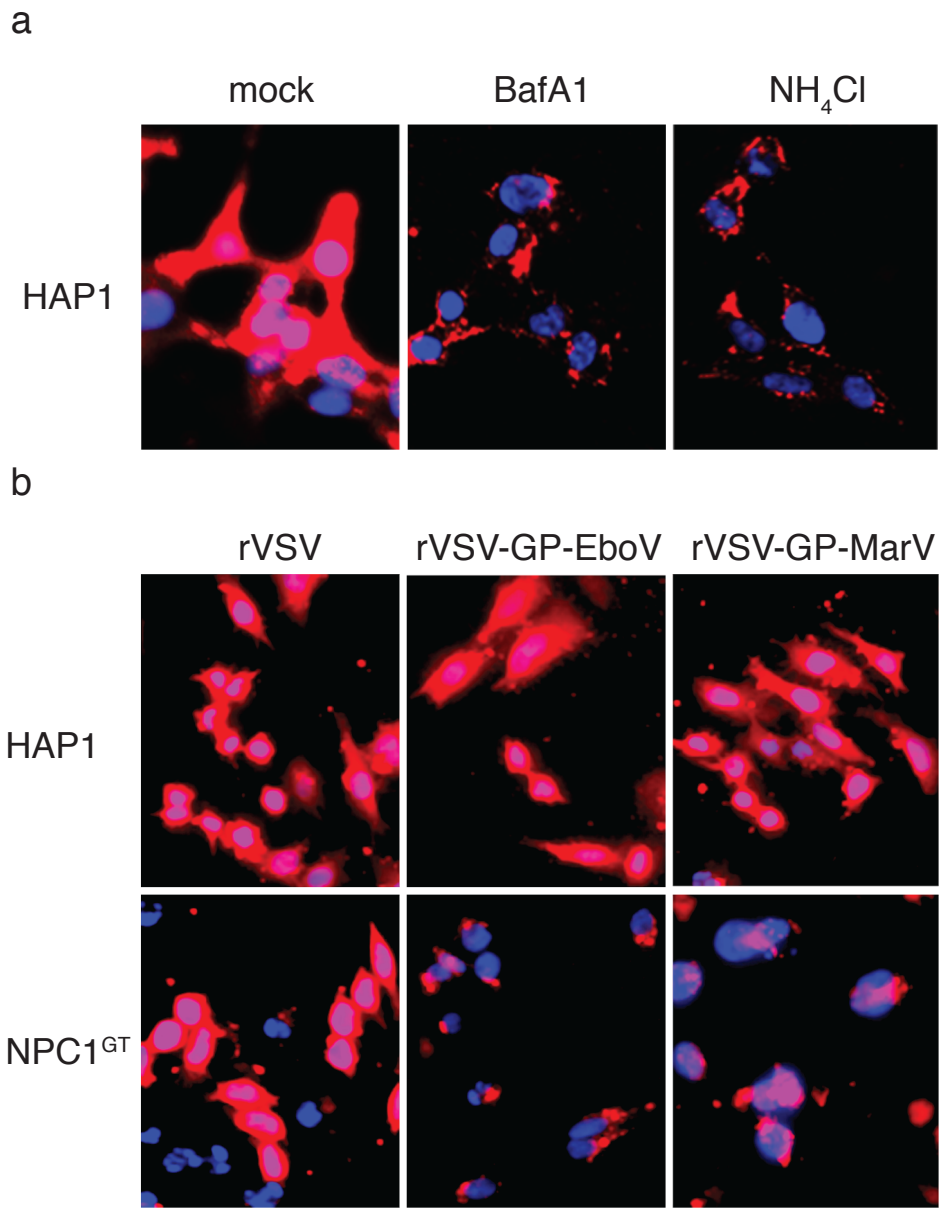

Supplemental Figure 15. Viral membrane fusion mediated by Ebola and Marburg glycoprotein requires NPC1. **a**, Wild type HAP1 cells were treated with puromycin (5 μg/ml) and inoculated with rVSV-GP-EboV in the presence or absence of bafilomycin A1 (bafA1; 100 nM) or ammonium chloride (NH4Cl; 20 μg/ml). Cells were fixed 3 h post inoculation and stained with VSV M antibody 23H12 as described in Methods. Successful fusion leads to the diffuse M staining (red) throughout the cytoplasm. Failure to fuse leads to discrete puncta of M staining as shown by bafA1 and NH4Cl. **b**, Wild type HAP1 cells and NPC1-deficient cells were treated with puromycin and inoculated with rVSV, rVSV-GP-EboV, or VSV-GP-MarV for 3 h and processed for VSV M staining as indicated above.

a

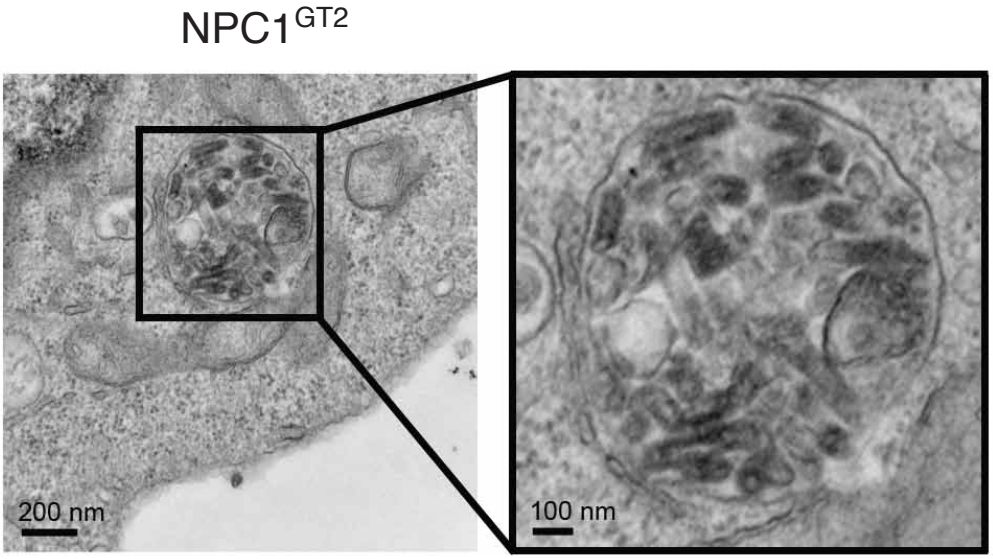

b

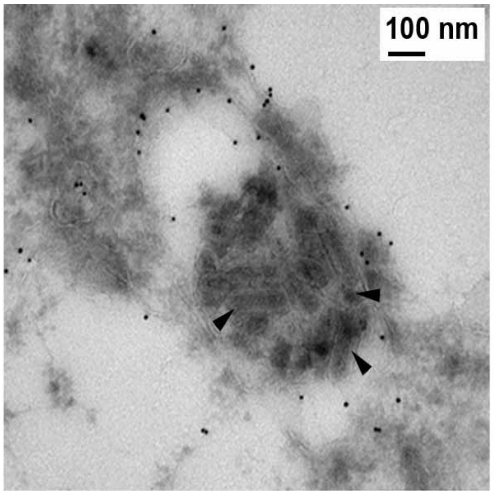

Supplemental Figure 16. Accumulation of rVSV-GP-EboV viral particles in vesicular compartments in NPC1-deficient cells. **a**, Electron micrograph of a second NPC1-deficient HAP1 clone infected with rVSV-GP-EboV. A large agglomeration of bullet-shaped VSV particles is visible within a vesicular (endosomal) compartment. The image was taken 3 h post-infection. **b**, NPC1-deficient HAP1 cells were inoculated with rVSV-GP-EboV and processed from cryo-immunogold electron microscopy as described in Methods. A representative image is depicted. Multiple viral particles (as indicated by the black arrows) can be detected in individual LAMP1-containing structures.

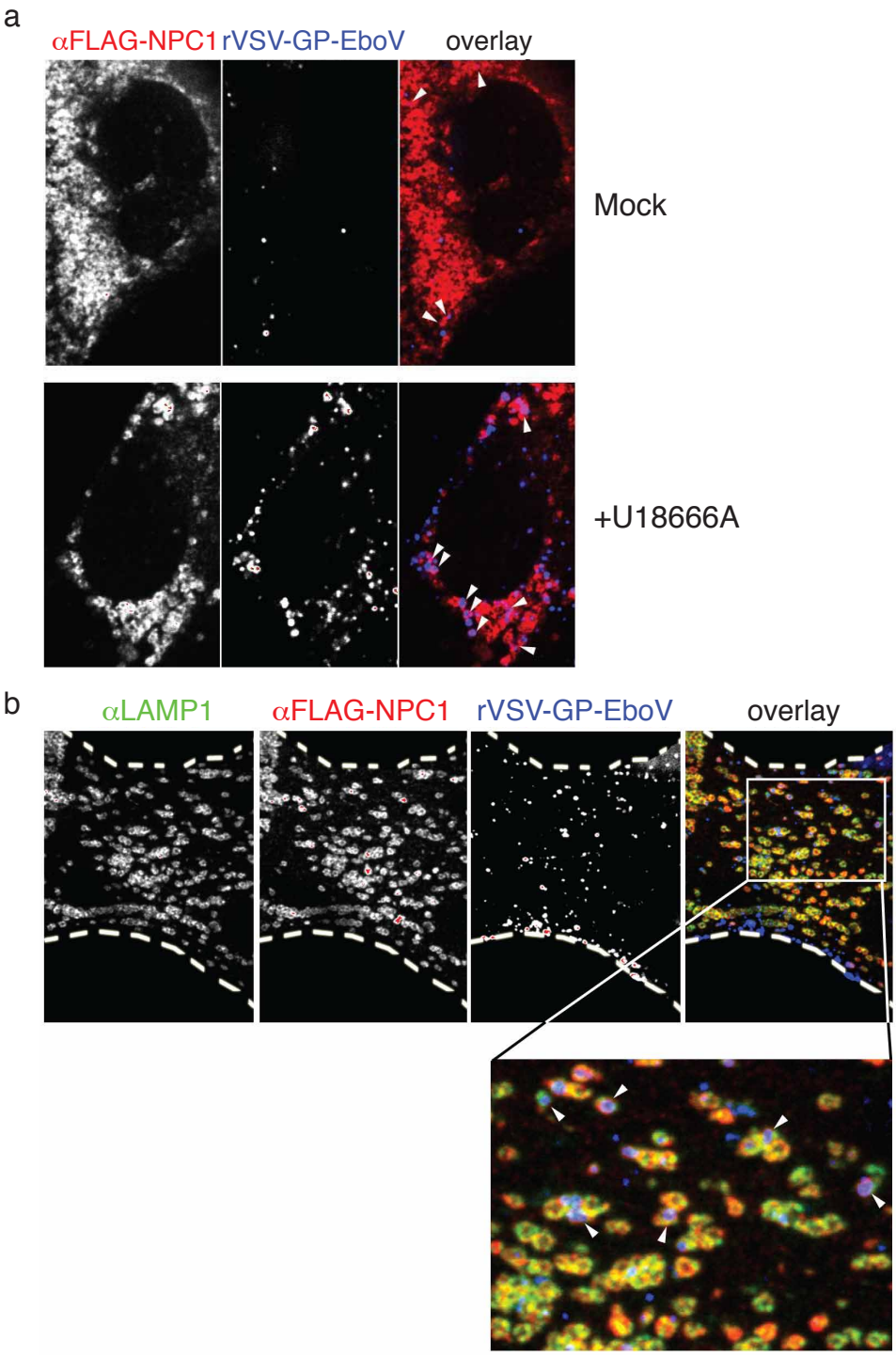

Supplemental Figure 17. Viral particles accumulate in NPC1- and LAMP1-positive endosomes in U18666A-treated cells. **a**, NPC1-mutant fibroblasts were transduced with a retrovirus directing the expression of NPC1 containing a Flag tag. Cells were exposed to Alexa 647-labeled rVSV-GP-EboV (blue) for 3 h in absence (mock) or the presence of 10 μg/ml U18666A. Subsequently, the cells were fixed with 4% PFA and immunostained with antibodies directed against the Flag tag (red). The degree of colocalization of NPC1-Flag with labeled rVSV-GP-EboV was determined on a pixel-to-pixel basis of individual regions of interest using the JACoP plugin in ImageJ software (mock; Pearson's coefficient: 0.094 ± 0.015, U18666A; Pearson's coefficient: 0.42 ± 0.14). **b**, In parallel, cells (exposed to Alexa 647-labeled rVSV-GP-EboV in the presence of 10 μg/ml U18666A) were stained with antibodies directed against the Flag tag (red) and LAMP1 (green) to visualize NPC1- and LAMP1-positive endosomal compartments (Pearson's coefficient: 0.894 ± 0.054).

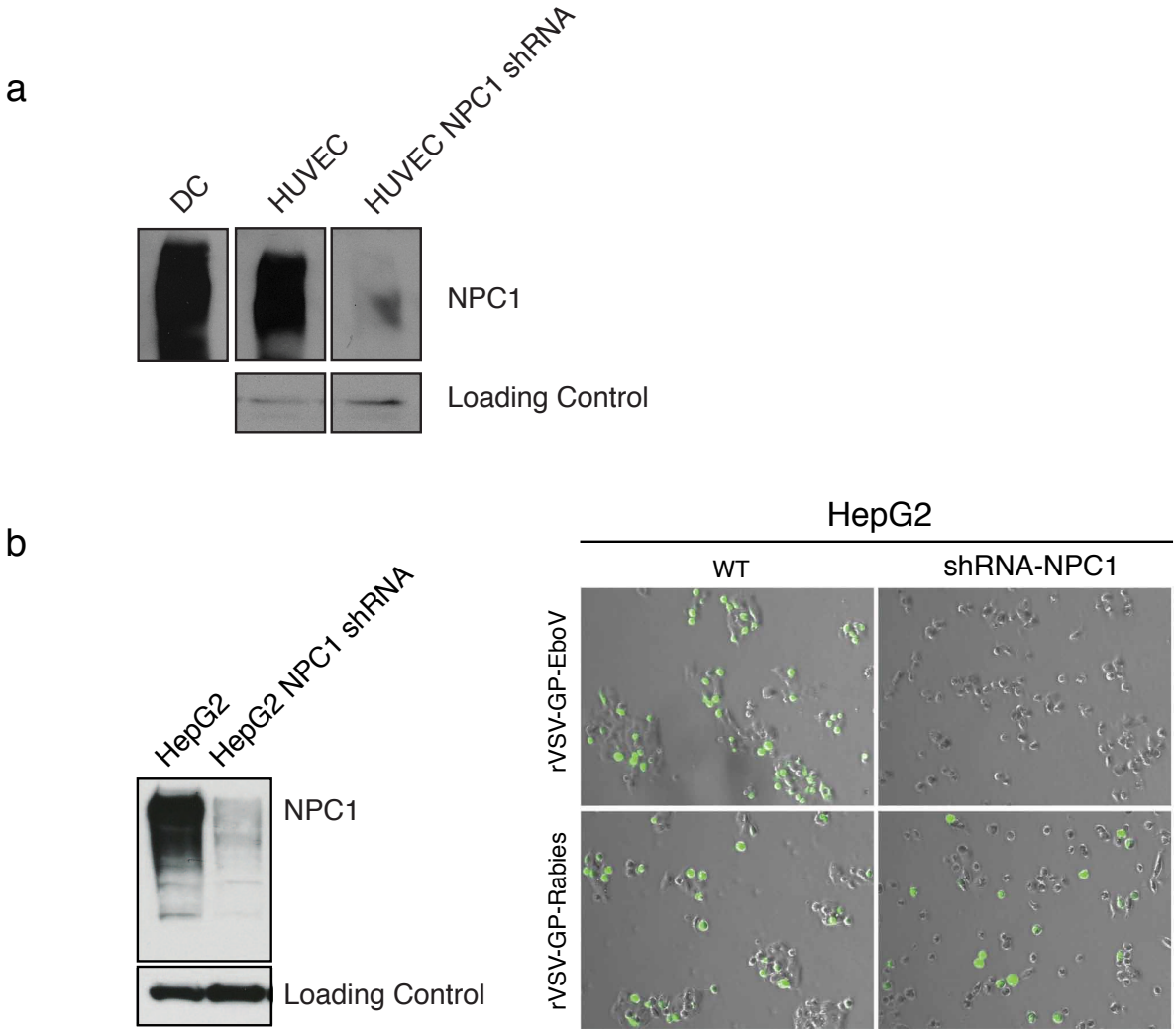

Supplemental Figure 18. NPC1 is expressed in human primary dendritic cells, endothelial cells, and a human hepatocyte cell line, and is necessary for viral infection of these cells mediated by the Ebola virus glycoprotein. **a**, Immunoblot analysis of primary human dendritic cells (DC) and endothelial cells (HUVEC) for expression of NPC1. HUVEC transduced with a lentivirus encoding an NPC1 shRNA express lower amounts of NPC1 relative to cells transduced with a non-targeting shRNA vector. Parallel samples were blotted for β–actin as a loading control. **b**, shRNA-mediated knockdown of NPC1 in HEP-G2 cells (left) impairs infection mediated by the Ebola virus glycoprotein but not by the rabies virus glycoprotein (right).

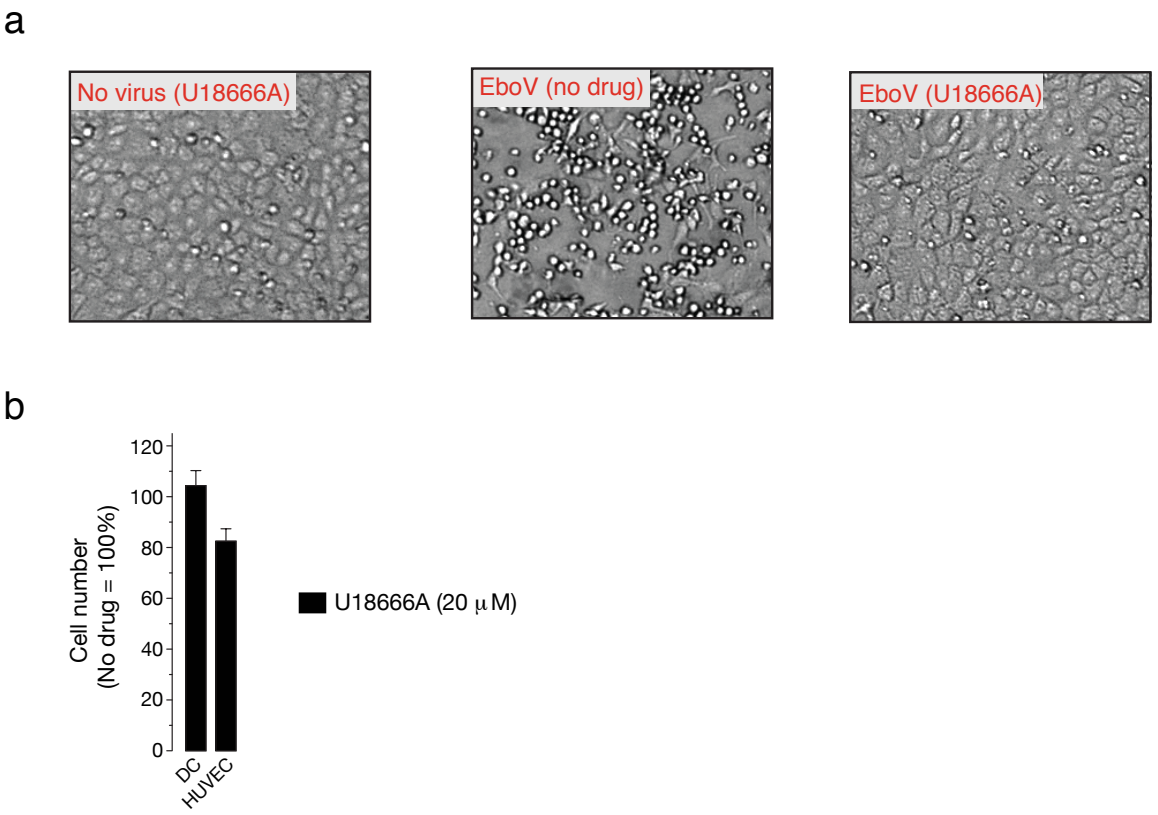

Supplemental Figure 19. U18666A is not cytotoxic to primary and cultured cell types under the treatment conditions employed in this study. **a**, Cells from the experiment in Figure 4c were photographed on day 4. U18666A was not markedly cytotoxic to cells even upon prolonged treatment. Moreover, virus-induced cytopathic effects were evident in untreated cells but not drug-treated cells infected with EboV. **b**, U18666A does not cause marked cytotoxicity in primary DC and HUVEC after 48 h of treatment.